Materials Chemistry and Physics 231 (2019) 75–86

Contents lists available at ScienceDirect

Materials Chemistry and Physics

journal homepage: www.elsevier.com/locate/matchemphys

Imidazole-supported silica one-pot processed nanoparticles to enhance toughness of epoxy based nanocomposites

Tankeshwar Prasad[a], Sudipta Halder[a,*], Siddhartha S. Dhar[b]

[a] Department of Mechanical Engineering, National Institute of Technology Silchar, Silchar, 788010, Assam, India
[b] Department of Chemistry, National Institute of Technology Silchar, Silchar, Assam, 788010, India

HIGHLIGHTS

- ISS nanoparticles was facilely prepared via one-pot co-condensation method.
- TEM micrograph demonstrates average particle size of ISS as ~8 nm.
- Composites with 1 wt% of ISS showed significant increment in K_{IC} and G_{IC}.
- The ISS/EP enhances the tensile strength and tensile modulus by ~45% and ~36%.

GRAPHICAL ABSTRACT

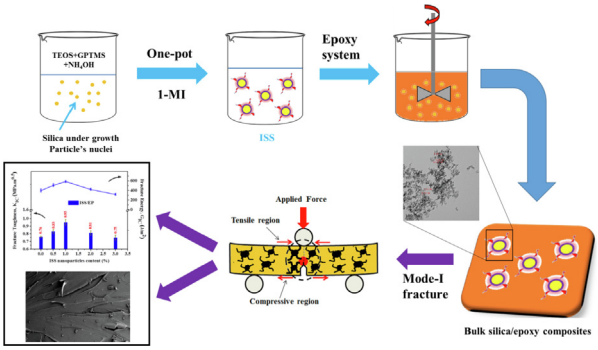

ARTICLE INFO

Keywords:
Silica nanoparticles
Sol-gel process
Nanocomposites
Ex-situ blending route
Mechanical properties

ABSTRACT

In this study, imidazole supported silica nanoparticle (ISS) was prepared from Tetraethyl orthosilicate (TEOS) precursor via co-condensation method. To warrant the chemical linkage of imidazole group to the silica surface, different spectroscopic characterization was performed. The microscopic investigation under TEM elucidates GMS/ISS particle size compared to as synthesized nanosilica (nS), which also endorses their surface modification. Further, ISS (0–3 wt %) was used to prepare epoxy nanocomposites. The ISS/EP enhances the tensile strength as well as the tensile modulus by ~45% (84 MPa) and ~36% (1.37 GPa) with respect to the neat epoxy (58 MPa and 1 GPa) respectively. Herein, the ISS nanoparticle uplifts the tensile performance of the epoxy nanocomposites at lower (1 wt %) filler content. To verify this result, further the dispersion study of ISS in epoxy system under TEM study was performed. A homogeneous distribution is observed at 1 wt % of ISS nanoparticles. In addition to that, Composites embedded with 1 wt % of ISS showed significant enhancement in toughness without sacrificing their stiffness properties. This noticeable improvement offered by ISS opens up the scope to use theses one-pot synthesized nanoparticles as toughness enhancer for highly brittle epoxy systems.

1. Introduction

From the past few decades, the nanoparticle in combination with polymer matrix enlarges the area of research for their applications in advanced composites. Among different polymers, DGEBA epoxy resin is a good choice as a matrix system for application of high performance composite owing to excellent thermal and mechanical properties like thermal stability, strength, stiffness and strong adhesion with

* Corresponding author.
E-mail address: sudiptomec@gmail.com (S. Halder).

https://doi.org/10.1016/j.matchemphys.2019.04.002
Received 6 February 2019; Received in revised form 28 March 2019; Accepted 1 April 2019
Available online 02 April 2019
0254-0584/

organically modified fillers [1–3]. It is used in various industrial area such as aircraft, defense, wind energy, locomotive and automotive etc. [4–6]. However, the intrinsic drawback of resin system is their stiffness and toughness, which is mostly dependent on crosslinking density. The too high cross-linking density of epoxy system results in brittle fracture even at low stress. To overcome such challenges, researcher across the globe tried many ways to enhance their tensile and fracture property without sacrificing their stiffness. One of the most effective approaches is to reinforced nano-fillers such as silica [7,8], ZnO [9–11], clay [12], carbon [13–17], TiO_2 [18], Al_2O_3 [19] and ZrO_2 [20] in the matrix system. From literature, it was found that using such nano-fillers infused resins improves their properties and lead tempting those challenges in many different fields. Most of works scrutinized the influence of organically modified silica to enhance their mechanical and other properties of epoxy system. As, nano sized silica particles have been extensively used as a reinforcement for epoxy resin due to their high modulus, specific surface areas, thermal stability along with low density, material cost and good abrasion resistance [21]. Hence, the overall performance of composites is basically depends on the surface chemistry of silica such as size, shape and wettability towards dispersion in matrix system. At present, out of the other inorganic nanofiller, SiO_2 nanoparticles tend to aggregate in highly viscous matrix system, which is a key challenge owing their hygroscopic nature (high polarity of particle's surface) and poor adhesion between nano sized SiO_2 particles and matrix system have restricted as the reinforcement [22]. In this regard, covalently functionalized nano-SiO_2 if incorporated in epoxy system can improve the dispersion quality as well as interfacial properties at the interface because it enriches its wettability [23]. From few reports, some epoxy and amino silane functionalized silica particles justifies as efficient reinforcement in epoxy system as the functional groups actively engage the curing process and thus, tailors the cross-linked networks of the epoxy system. For instant, C. Alzira et al. [24] reported use of epoxide group modified nano silica in epoxy system and evaluated the interfacial effect on T_g and thermal properties of epoxy system. They highlighted improvement in T_g due to better dispersion in comparison with bare silica. Similarly, H. Behniafaret al [25] reported effect of amine modified nanosilica on viscoelastic response of epoxy resin system. The storage moduli value of modified nanocomposites is about four times higher (0.94 GPa) than that of neat epoxy network (0.18 GPa). The storage modulus (*E"*) and thermal stability of composites containing amino functionalized silica nanoparticles (5 wt %) demonstrated superior behavior relative to the unmodified composites. Han et al. [26] reported the fracture toughness of epoxy nanocomposites by using amino and epoxide groups functionalized commercial nanosilica. The K_{IC} value of amine functionalized epoxy nanocomposites improves 25% (1.15 MPa $m^{0.5}$) with respect to neat epoxy (0.92 MPa $m^{0.5}$) while epoxy functionalized nanocomposites enhancement 36% (1.25 MPa $m^{0.5}$) at 2 wt %. Further, M. Conradi et al. [27] reported mechanical properties of nanosilica-reinforced epoxy nanocomposites. They demonstrated 11% (141 MPa), 15% (3 GPa) and 38% (0.91 MPa $m^{0.5}$) enhancement in tensile strength, tensile modulus and fracture toughness property of epoxy matrix at 0.5 vol % of nanosilica compare to pure epoxy (127 MPa, 2.60 GPa and 0.66 MPa $m^{0.5}$ respectively). So far, most of the work on SiO_2/epoxy system has primarily focused on conventional amine based hardener, whereas the research on anhydride based hardener is hardly been reported. In fact, using anhydride based epoxy system has some additional benefit such as low viscosity, high pot life and excellent thermal stability over amine based epoxy systems. These profits are highly adorable for tailoring high performance composites structure for advance applications. Furthermore, the curing kinetics pathway of anhydride cured epoxy systems can be tailored via imidazole modified nano filler to suit for different applications. Recently, W. Liu et al. [28] reported the synchronous reinforcing and catalytic effects of imidazole modified graphene in anhydride based epoxy system. They demonstrated the tensile strength and Young's modulus of composites (0.4 wt %) were enhanced by 97% and 12% respectively compare to neat epoxy. In some other work, Q. Lyu et al. [29] reported the reinforcing and catalyzing effect of imidazolium ionic liquid modified GO in the same system, They found increment of 12% in flexural strength (141 MPa), 26% in flexural modulus (5 GPa), and 52% in impact strength (18 kJ/m^2) compared to control epoxy system. Similarly, Zhang et al. [30] reported the influence of supported ionic liquid modified silica on mechanical properties of amine based epoxy system. They achieved maximum enhancement of ~13% in tensile strength (52 MPa), ~20% in flexural strength (84 MPa), ~9% in flexural modulus (2.32 GPa) and ~17% in impact strength (19.2 kJ m^{-2}) with respect to unmodified epoxy system at 30 wt %. This gives the essence of scrutinizing imidazole supported silica particle (ISS) for the use as epoxy curing agent to improve mechanical and fracture properties.

In the present study, we demonstrated how the introduction of ISS in anhydride based epoxy system can affect the mechanical and fracture properties of composites with respect to unmodified epoxy system. In order to obtain better dispersion of ISS in epoxy system, we develop a new method for surface modification of nanosilica [31]. Investigation was also done to pinpoint the factors that are responsible for enhancement in mechanical and fracture properties of imidazole supported silica reinforced epoxy (ISS/EP) nanocomposites. Identification of failure mechanism of nanocomposites is done in detail using fractography analysis.

2. Experimental details

2.1. Materials

In the present work, Tetraethyl-orthosilicate (TEOS, purity 98%)was used as a precursor and ammonia solution (25% NH_3in water)as a catalyst obtained from Merck Specialties Private Limited, Mumbai, India. (3-Glycidyloxypropyl) trimethoxysilane (GPTMS ≥ 98%) used as coupling agent purchased from Alfa Aesar India Pvt. Ltd. Hyderabad, India. Di-glycidylether bisphenol-A (DGEBA) epoxy resin (Araldite LY556), anhydride based hardener (Aradur HY 906) and 1-methyl imidazole as an accelerator (DY 070) supplied by Huntsman India Pvt. Ltd., India was used as epoxy system.

2.2. Synthesis of surface modified silica nanoparticle

The nanosilica (nS) particle was synthesized using sol-gel method [32]. Further, the GPTMS modified silica nanoparticle (GMS) was synthesized by co-condensation via the sol-gel process. In a typical procedure, 4 ml (0.50 M) of TEOS was added to 250 ml beaker containing 30 mL of ethanol, 400 μl (10 wt % of TEOS) of GPTMS and 2 ml (3 M) of deionized water. The homogeneous solution was vigorously stirred and 1.4 ml (1 M) of ammonia solution is added drop wise. The reaction was allowed to proceed under moderate stirring at room temperature for another 5 h. The white milky gel is formed, which was separated by centrifugation and repeatedly washed with ethanol and deionized water, and finally the powders were dried at 90 °C for 24 h in a vacuum oven.

The imidazole supported silica particle (ISS) was synthesized using one-pot process via co-condensation method. In a typical procedure, 4 ml (0.50 M) of TEOS and 2 ml (3 M) of deionized water were added to round bottom flask containing 30 mL of absolute ethanol and stirred vigorously for 30 min at room temperature to prepare homogenous solution. Subsequently 4 ml (1 M) of 28% NH_3 solution was added via pipette and stirred for next 4 h. Consecutively, 400 μL GPTMS (10 wt % of TEOS) using micro-pipette and 2 g (25 mmol) 1-methyl imidazole was added to the above reaction mixture purging with dry nitrogen, and continue stirring for another 8 h. The ISS nanoparticle was purified and separated by centrifugation and they were thoroughly washed by ethanol until clear transparent solution was detectable in the centrifuge tube. Then they were dried at 90 °C under vacuum for 8 h.

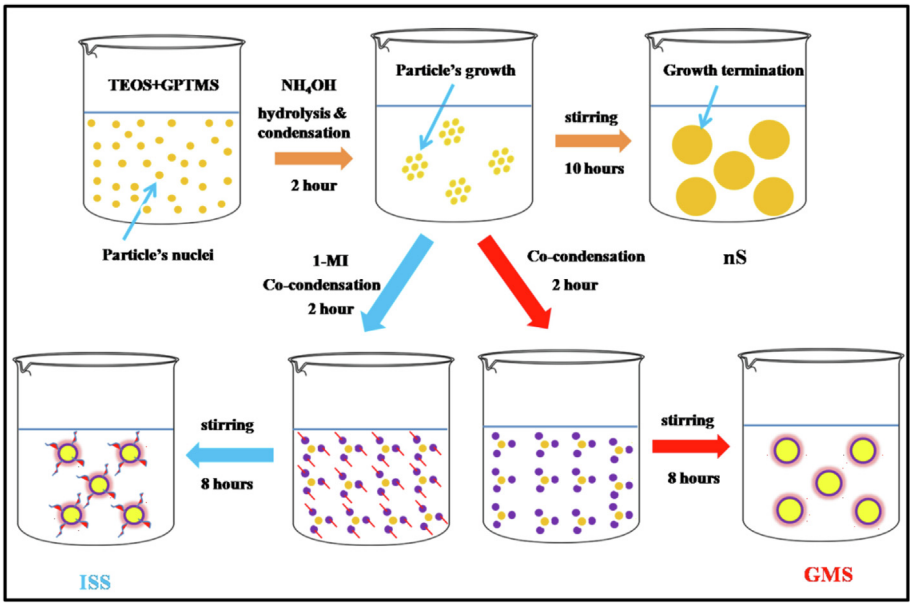

Fig. 1. Schematic representation for surface functionalization of silica nanoparticles via one-pot sol-gel route.

2.3. Preparation of silica/epoxy nanocomposites

In present work, silica/epoxy nanocomposites were prepared by varying content (0–3 wt %) of the variants (nS, GMS and ISS) embedded into hardener and thoroughly mixed using high shear impeller agitation at 1400 rpm for 10 min followed by acoustic cavitation (via probe sonication) for another 30 min. The dispersion of nano-SiO_2 into epoxy system was performed by ultrasonic probe sonicator (Q-Sonica, Newtown, CT, USA) with maximum output power of 700 W (Frequency: 20 kHz, amplitude: 70%) under dual mode mixing. The blend temperature was constantly monitored and maintained at room temperature by thermocouple using circulating cold water around the blend enclosed with Teflon made jacket via water bath chiller to avoid degradation. Then, stoichiometric amount of epoxy resin and initiator D070 (weight ratio of epoxy: hardener: initiator is 100:95:2) was added to the above mixture and continued mixing for another 5 min to obtain a homogeneous mixture followed by degassing under vacuum for 30 min. Then, the mixture was poured into a silicone rubber mold and kept in vacuum oven with two stage curing system which includes precuring at 120 °C for 2 h and post cured at 160 °C for 8 h.

2.4. Method of characterizations

The surface properties of nS/GMS/ISS nanoparticles were investigated by FTIR spectra using Bruker Vertex 80 spectrometer, Germany in the range of 4000 to 400 cm^{-1}wave number. The samples were bound in the pellets form using pallet press with KBr. X-ray photoelectron spectrum (XPS) measurement was performed on an AXIS Supra (Kratos Analytical, UK (SHIMADZU group)) with an aluminum monochromatic (Al-Kα) 600 W X-ray source (1486.6 eV). Thermogravimetric analysis (TGA) was performed on a thermal analyzer (NETZSCH STA 449 F3 Jupiter, Germany) using 10 mg of samples in a temperature range of 30 to 800 °C with heating rate of 10 °C/min under N_2 gas purging (30 ml/min) on Al_2O_3 sample pan. The ^{29}Si Nuclear magnetic resonance (^{29}Si NMR, 500 MHz) signals were recorded using Bruker Instrument (Bruker Advance III, Billerica, MA, USA) in DMSO solvent (hydrogenated). Transmission electron microscopy (TEM) was performed on a JEOL (JEM 2100, Japan) with an operating voltage of 200 kV to predict the particle shape and size. The samples were prepared by sonicating silica particles (0.05 mg/ml) in absolute ethanol for 30 s. Subsequently, putting one drop of the suspension on amorphous carbon-coated copper grid followed by evaporating solvent. The dispersion analysis for epoxy nanocomposites was done on samples prepared by using programmable spin coating (model: Spin NXG-P2, make: APEX Instruments, Russia) process. For the spin coating process, the ISS/epoxy mixture were deposited on the overhead polymer substrate (O·H.P. sheet) and spin coated at the rate of 5000 rpm for 30 s followed by second spin-up rate at 9000 rpm for 60 s. Then the produced composites thin film was cured at 80 °C for 2 h to solidify the nanocomposites mixture. The specimens of 1 cm^2 in size were prepared using low speed diamond disc cutter followed by grinding and polishing. Finally the TEM was used to predict the microstructure of particles dispersion state in epoxy resin system. The tensile and three point notched bend (SENB) test of nanocomposites were performed using computerized universal tensile machine (INSTRON, Model 5969, USA) at a cross-head speed of 1 mm/min. The tensile samples were prepared in accordance with ASTM D638 (type-V) followed by grinding and polishing. The fracture property of nanocomposites was demonstrated by following the ASTM D5045 standard. According to standard test procedure [33], the K_{IC} and G_{IC} were calculated equations (1)–(3).

$$K_{IC} = \frac{6P}{BW} \times \sqrt{a} \times Y \tag{1}$$

Where Y is the shape factor determine by equation (2):

$$Y = \frac{1.99 - \frac{a}{W}(1 - \frac{a}{W})(2.15 - 3.93(\frac{a}{W}) + 2.7(\frac{a}{W})^2)}{(1 + 2\frac{a}{W})(1 - \frac{a}{W})1 - \frac{a}{W})^{\frac{3}{2}})} \tag{2}$$

Here, P is maximum applied force, W is width, B is thickness and 'a' is the depth of notch of the specimen.

$$G_{IC} = K_{IC}^2[(1 - \upsilon^2)/E] \tag{3}$$

Here, υ is Poisson's ratio of composite material and is equal to 0.33; E is tensile elastic modulus, K_{IC} is fracture toughness and G_{IC} is fracture energy.

3. Results and discussion

3.1. Reaction mechanism and morphological investigation of GMS and ISS nanoparticles

The scheme depicting plausible reaction mechanism for surface functionalization of silica nanoparticles via one-pot sol-gel route to

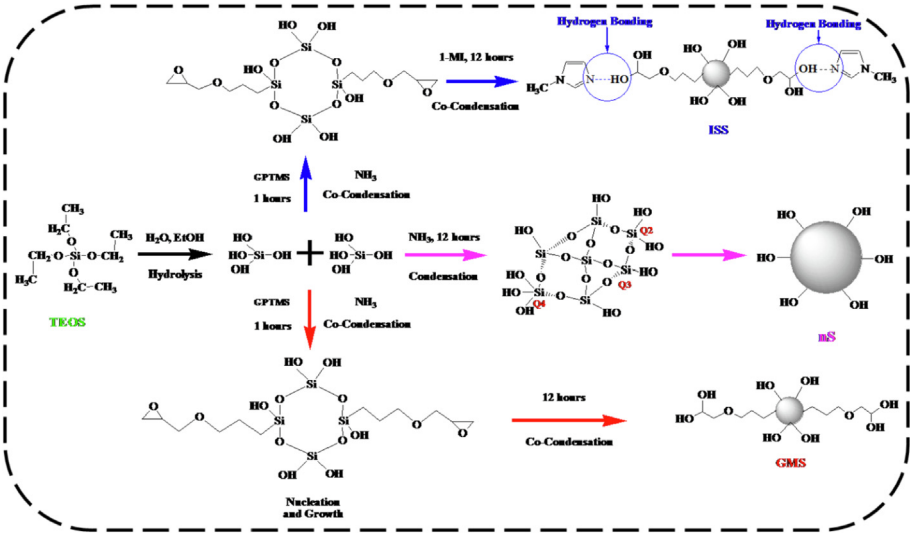

Scheme 1. Proposed reaction mechanism for synthesis of nS, GMS and ISS nanoparticles.

produce GMS and ISS is shown in Fig. 1. In the typical process of GMS nanoparticle synthesis firstly a fixed molar ratio of TEOS and water was mixed with pre-determine quantities of ethanol. During this process, TEOS was first hydrolyzed to ethoxyl groups (−*Si*-OEt) to produce the monomer of silanol groups (−*Si*−OH). Then, the condensation between two silanol groups occurs after additions of NH_3 to generate branched siloxane clusters (Si-*O*-Si bonds) under controlled nucleation and growth of particles followed by growth termination. In this study, under high NH_3 concentration, the growth mechanism of silica nanoparticles follows the "monomer addition" model [34].

This model is true for the formation of nanosized silica particles at experimental condition, when high concentration of NH_3 is used. It was found that the reaction time decreases significantly as NH_3 concentration (> 0.90 M) is increased. In view of the above, TEOS hydrolysis involves the formation of penta-ethoxyl group via nucleophilic substitution reaction. This is because of the faster rate of hydrolysis under high NH_3 concentration. Hence, hydrolysis rate accelerates the conversion of large amount of silanol groups to form more ethoxyl groups, which is attributed to the increase in Si^+ atoms that reduces steric intermolecular interaction of ethoxyl groups that is expected to favor more nucleophilic attack for the formation of silanol groups. In the case of GMS, as schemed in Fig. 1, the growth mechanism of particles can be correlated with the "aggregation only" model [35]. In the first step, primary silica particles are formed after ammonia addition in the reaction mixture. The second step involves the primary particles transformation into oligomers by the co-condensation of TEOS and GPTMS. During the reaction, first of all methoxyl groups of GPTMS are hydrolyzed in the presence of excess water via self-condensation reactions and form hydrolyzed silane. Later, this hydrolyzed silane molecules are anchored among each other through covalent bond and release water molecules. Thus, GMS particles are expected to form diol species via a combination of poly-condensation and the co-condensation reactions between TEOS and ring opened epoxide groups of GPTMS. Since, the poly-condensation reactions are expected to slow down the poly-condensation of silica and the epoxy opening reactions under highly basic conditions. The relative rate of hydrolysis and condensation can be controlled by choosing proper amount of GPTMS with respect to TEOS to tailor a final chemical structure of GMS. The disappearance of epoxy end-groups of the GPTMS molecules during formation of GMS was explained in details by P. Innocenzi at el [36]. They reported the reactions in highly basic conditions (pH ~14) of GPTMS organic molecules in presence of TEOS by liquid state ^{13}C NMR. In the study, they marked different C-atoms in GPTMS from 1 to 6. In particular, C in positions 5 and 6 are assigned to the epoxy end group and was monitored the opening reactions during reaction process. They observed the ring opening is not a fast process under highly basic conditions and appears to proceed with an almost constant rate with the reaction time, this was confirmed by the decrease of epoxy signals 6 (43 ppm) and 5 (52 ppm). A similar trend was observed for carbon signals at 64, 69, 70 ppm, they start to appear after one day of reaction and steadily increase in intensity with aging time. The couple of signals at 64 and 70 ppm were assigned to diols formation by hydrolytic opening of the epoxy end-groups of the GPTMS molecules. Further, the reaction growth mechanism for synthesis of ISS nanoparticles (Fig. 1) is very similar to the synthesis of GMS nanoparticles following the "aggregation only model".

The reaction was performed via co-condensation reaction of TEOS and GPTMS in presence of imidazole. Herein, imidazole catalyst acts as anions that might potentially behave as an electrophile, which accelerates the co-condensation reaction between TEOS precursor and GPTMS co-precursor. Thus, inorganic polymerization between TEOS and GPTMS and organic polymerization between GPTMS and 1-methyl imidazole was taken place. Further, at the end of reaction process, the major functional group on the surface of pure silica (nS) was examined by using FTIR and ^{29}Si NMR spectrometer (Fig. 4(a and b)), which was discussed later of section 3.2 in detail. On the basis of these results obtained from spectroscopic analysis of nS, GMS and ISS nanoparticles, the final chemical structure of ISS [37] was tailored as shown in Scheme 1.

The main purpose of studying scanning electron microscope of nanoparticles is to observe the morphologies of silica nanoparticles before and after modification. However, the nanoparticles changed to nanosize cluster by aggregation, in this case, it is impossible to observe the existing clusters in dispersion state of particles. According to SEM images shown in Fig. 2, we can observe that the size in SiO_2 nanoparticles do not change before and after modification due to formation of large aggregation of particles under the influence of hydrophilicity. However, to obtain the clear distinguished among size of each particle, further TEM analysis was performed. On the other hand, the morphologies of silica particles before and after modification were analyzed under SEM as shown in Fig. 2. As expected, the morphology of sol-gel (modified Stöber method) derived functionalized and unfunctionalized nanoparticles are spherical and homogeneous. The morphological investigation under SEM demonstrates higher level of silica nanoparticle aggregation even after surface modification, possibly due to hygroscopic nature of silica.

The size of the three nanoparticles nS, GMS and ISS are quite different (Fig. 3) due to the different hydrolyzation and condensation rates

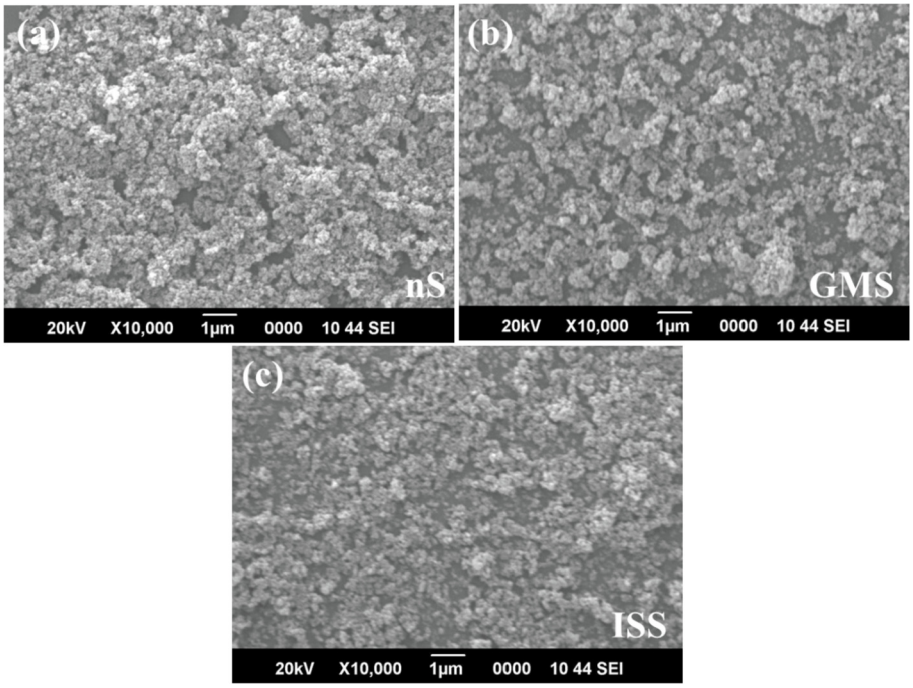

Fig. 2. SEM micrographs of (a) nS (b) GMS and (c) ISS nanoparticles.

of TEOS, between GPTMS/TEOS molecules and the TEOS/GPTMS/1-MI organic moieties respectively. The variation in particle size of nS, GMS and ISS was further obtained from the TEM investigation as shown in Fig. 3. TEM micrograph demonstrates particle size of nS as ~170 nm, whereas for GMS it was ~14 nm and for ISS it was ~8 nm respectively. The reduction in particle size of GMS compared to nS is attributed to controlled hydrolysis rate of TEOS and GPTMS, whereas further reduction in particle size for ISS is achieved by controlling the degree of condensation rate between GPTMS and imidazole. Since, Imidazole is nucleophilic in nature, the imidazole group (pyridine-nitrogen) increases the catalysis resulting in strong ionic interactions between imidazole and the epoxide group of GPTMS [38]. Here, the reduction in particles size of both GMS and ISS in comparison to nS can be better explained by the diffusion and reaction kinetics model [39]. This model suggests higher Gibbs free energy of a supersaturated reaction solution because of the addition of organic moieties. The free energy for nucleation is mainly depends on the radius of nuclei as well as volume and surface free energy. So during the sol-gel process, the particle growth is a function of time, concentration, temperature, and viscosity of reaction mixture etc. [40]. For the uniform particle growth, it is best to have a short nucleation time so that during subsequent particle growth, all the nuclei are allowed to grow for an equal amount of time. In this work, as shown in Fig. 3 (b) and (c), there is reduction in particle size. The addition of organic moieties into the reaction mixture in a shorter time resulted in covalent or ionic interaction between each nuclei and the functional groups, which we are expecting to, restrict further growth of the nuclei. In the case of GMS synthesis, the surface of silica was grafted covalently with the GPTMS. On the other hand, the surface modification of silica with imidazole moieties consists of two step reaction. In the first step, covalent interaction between TEOS precursor and the GPTMS and in the next stage ionic interaction between the hydroxyl groups terminated GPTMS with the imidazole (as shown in reaction Scheme 1).

3.2. Investigation of functional group attachment on the nano silica

The major functional group on the surface of pure silica (nS) was firstly examined by using FTIR spectrometer and the obtained result is shown in Fig. 4 (a). The IR peak of nS shows the narrow absorption peak at ~3400 cm^{-1}, which is attributed to H-bonded from silanol OH group [41]. The peak at ~1600 cm^{-1} can be assigned to bending vibration modes of physically adsorbed water molecules. The characteristic peaks ~1090 and 800 $cm^{-1}$are related to the symmetric and asymmetric stretching vibration of Si-*O*-Si bond. The peak at ~460 cm^{-1} and ~567 cm^{-1} are assigned to Si-*O*-Si out of plane racking (bending) and asymmetric stretching modes. This observation confirms no presence of unreacted TEOS that can appear after synthesis of the nS nanoparticles via sol-gel method [42].

In the case of GMS as well as ISS, new sharp absorption peak is observed at ~2878 cm^{-1} and ~2950 cm^{-1} respectively corresponding

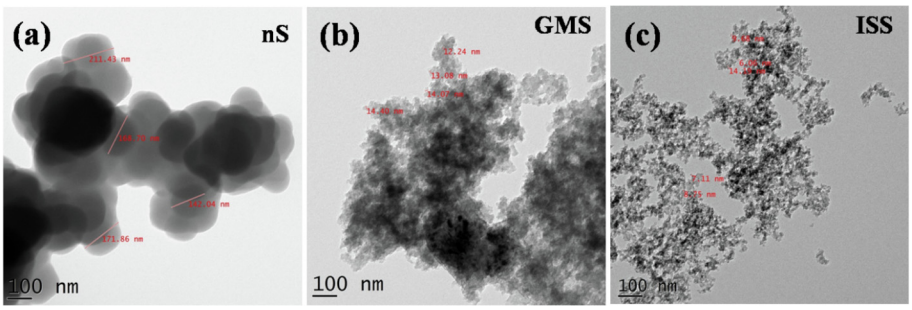

Fig. 3. TEM micrographs of (a) nS (b) GMS and (c) ISS nanoparticles.

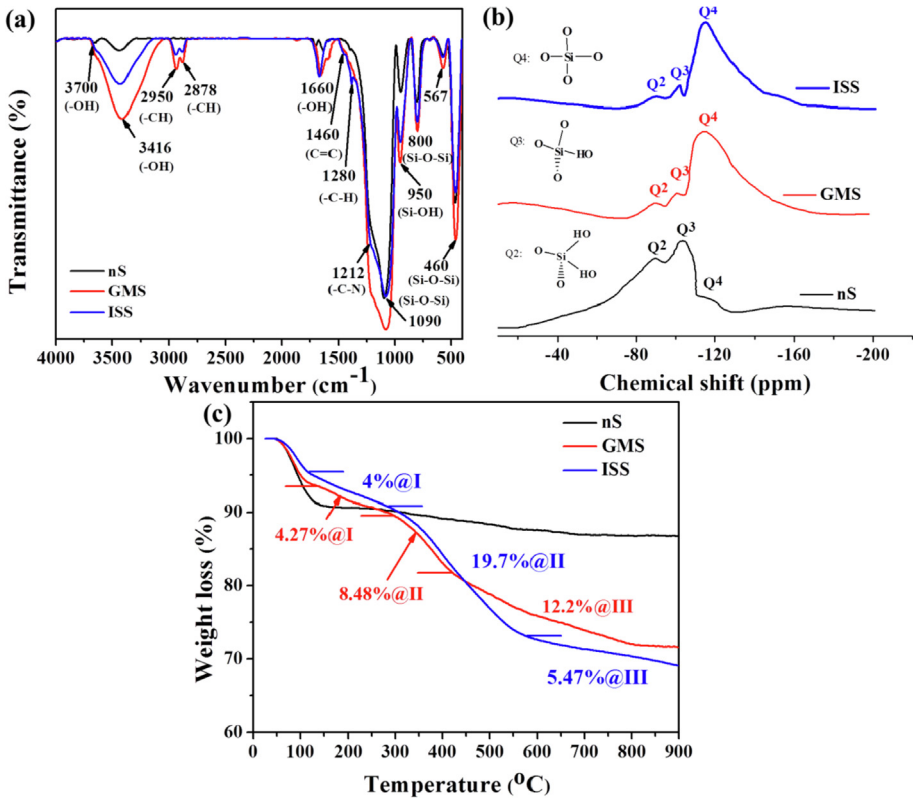

Fig. 4. (a) FTIR spectra of nS, GMS and ISS nanoparticles (b) The ^{29}Si NMR spectra showing signal characteristics of nS, GMS and ISS nanoparticles (c) TGA curves of nS, GMS and ISS nanoparticles.

to the symmetric and asymmetric stretching vibration mode of C-H band. For GMS, peaks at ~1280 cm^{-1} and ~910 cm^{-1} is likely to be present corresponding to the epoxy ring breathing and the epoxy asymmetric bending (C-*O*-C) respectively. The absence of these bands for GMS provides a strong evidence for opening of the epoxide ring of GPTMS molecules in presence of NH_3 as catalysis from TEOS [43]. The broadening of peaks corresponding to ~3416, ~950 and ~800 cm^{-1} for GMS with respect to nS indicates the hydrolysis of TEOS and GPTMS in the presence of water molecules. For ISS, the further broadening of peak at ~1090 cm^{-1} indicates the faster condensation rate of GPTMS in presence of 1-methyl imidazole as we have schemed in Scheme 1. Furthermore, new absorption peak at ~1212, ~1280 and ~1460 cm^{-1} for ISS is ascribed to C-N asymmetric stretching, C-H asymmetric stretching and C=C symmetric stretching respectively from imidazole [44]. The presence of these bands confirms the attachment of imidazole on the surface of nS. The chemical structure of nS, GMS and ISS was evaluated based on the results obtained from ^{29}Si-NMR as shown in Fig. 4(b). From the spectra of GMS as well as ISS, the observed major three characteristic peaks demonstrates chemical shift corresponding to the bi-functional (Q^2), tri-functional (Q^3) and tetra-functional Si-O units (Q^4). This is ascribed to the hydrolysis and condensation reaction of TEOS and GPTMS in presence of ammonia and imidazole. The signals at −89 ppm, −102 ppm and −111 ppm are assigned to Q^2 [$Si(OH)_2$] Q^3 [Si(OH)] and Q^4 (SiO_4) chemical species as listed in Table 1.

The signals at Q^2 is found increased by 1 ppm while the signal Q^3 is reduced by 3 ppm and the signals at Q^4 is increased by 2 ppm for GMS with respect to the nS. However, in the case of ISS only signal at Q^4 is found increased by 4.6 ppm, confirming the condensation of both silane compounds. The small peak at Q^3 decreases significantly with respect to nS for both GMS and ISS, indicating a high degree of condensation between GPTMS and TEOS during the synthesis process [45]. Again on the basis of these results, the final chemical structure of ISS as proposed in Scheme 1 is confirmed. The thermal degradation analysis of the nS, GMS and ISS was performed under TGA as shown in Fig. 4(c). From TGA plots, a three step weight loss of GMS and ISS particle is found. The weight loss for nS was observed within the range of 136 °C to 546 °C by ~5.5%. This weight loss is attributed to the volatilities of OH groups. In case of GMS and ISS, weight loss under first stage occurred in a temperature range of 117–286 °C and 141–294 °C corresponding to ~4% and ~4.27% respectively. This is associated to the removal of physically absorbed moisture and water on the surfaces of GMS and ISS. Mass loss under second stage within the range of 286–580 °C (19.7%) for GMS and 294–413 °C (8.48%) for ISS respectively could be attributed to the degradation of methyl group moiety from GPTMS and imidazole. Finally in the third stage, weight loss was observed in the range of 580–896 °C (5.47%) for GMS, 413-803 °C (12.2%) for ISS respectively is attributed to all losses of carbon, oxygen and nitrogen from the surface of GMS and ISS. A noticeable increased weight loss of GMS and ISS than that of nS, indicates the presence of functional organic moieties on the facial portion of nS [46]. In addition, the grafting density of GPTMS and Imidazole moiety on the surface of GMS and ISS nanoparticle was estimated within the temperature range of 300 to 800 °C by the following equation (4) and is listed in Table 2 [47].

Table 1
The signal characteristics peaks response of nS, GMS and ISS nanoparticles under^{29}Si-NMR spectra.

Sample code	Q^2	Q^3	Q^4
nS	−89	−103	−111
GMS	−90	−100	−113
ISS	−90	−101.8	−114.6

$$\textit{Grafting density}\ (\textit{mmol/g}) = \left[\frac{W_{300-800}}{100 - W_{300-800}}\right] \times \left(\frac{1000}{M}\right) \quad (4)$$

Table 2
Grafting density of organic moieties on the surface of ISS was estimated by TGA.

Sample code	Mass loss at 300 °C (%), W_{300}	Mass loss at 800 °C (%),W_{800}	$W_{300} - W_{800}$ (%)	Silane Grafting (Wt %)	Silane Grafting (mmol/g of nS)
nS	90	87	3	0	0
GMS	89	72	17	14	0.69
ISS	90	70	20	3	0.37

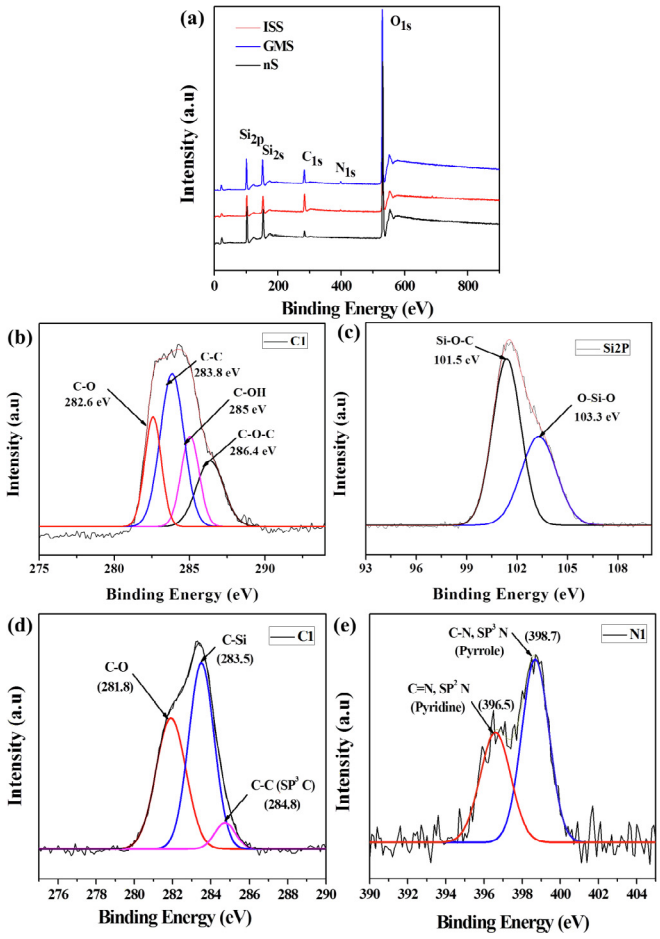

Fig. 5. (a) X-ray-photoelectron spectroscopy (XPS) broad scans for nS, GMS and ISS (b) Deconvoluted curve-fitting of GMS for XPS core-level of C1 (c) Deconvoluted curve-fitting of GMS for XPS core-level of Si2P (d) Deconvoluted curve-fitting of ISS for XPS core-level of C1 (e) Deconvoluted curve-fitting of ISS for XPS core-level of N1.

Where,$W_{300\text{-}800}$ is weight loss of silica in a temperature range of 300–800° and M (g/mol) is the molecular weight of the grafted silane molecules.

The surface functional group attachment for nS, GMS and ISS nanoparticle is finally investigated under XPS (survey and high resolution spectrum) as shown in Fig. 5(a–e). From Fig. 5 (a), the binding energies at peaks around 100, 150 and ~530 eV is related to the Si_{2p}, Si_{2s}, and O_{1s} respectively corresponding to the characteristic of nS [48]. After modification of nS with GPTMS, peaks with binding energy ~283 eV is observed, which is assigned to C_{1s}, justifying the presence of GPTMS moieties on the surface of silica [49]. Similarly, modification of nS with imidazole through the linkages of the GPTMS, peaks with binding energy ~283 and 399 eV is observed, which is assigned to C_{1s} and N_{1s} respectively, which is in good agreement with the presence of imidazole moieties on the surface of silica [50]. After deconvolution curve-fitting of C_{1s} for GMS four main peaks at binding energies 282.6, 283.6, 285 and 286.4 eV is observed. These peaks are corresponds to C-O, C-C, C-OH and C-*O*-C bonds respectively (Fig. 5 (b)). The Si_{2p} deconvolution of GMS demonstrates two major peeks at binding energies 101.5 and 103.3 eV (Fig. 5 (c)), which corresponds to two atomic bonds of Si-*O*-C and O-Si-O groups, respectively. This observation justifies the presence of carbon and silicon atoms attached on the structure of the nS in the form of GPTMS moiety. In similar way, the deconvolution curve-fitting of C_{1s} for ISS three main peaks at binding energies 281.8, 283.5 and 284.8 eV is observed. These peaks are corresponds to C–O, C-Si and C–C bonds (sp^3 hybridized carbon atoms) respectively (Fig. 5 (d)). The N_{1s} deconvolution of ISS demonstrates two major peeks at binding energies 396.5 and 398.7 eV (Fig. 5 (e)), which corresponds to two atomic bonds of C═N pyridine and C–N pyrol groups of nitrogen atoms, respectively from imidazole. This observation justifies the presence of two nitrogen atoms attached on the structure of the nS in the form of imidazole moiety.

3.3. Tensile properties of nanocomposites

The tensile performance of nanocomposites prepared with the varying content (0–3 wt %) of bare and modified silica nanoparticles is shown in Fig. 6 (a). The tensile strength and tensile modulus of neat epoxy system is found as ~58 MPa and ~1 GPa respectively. For the nS

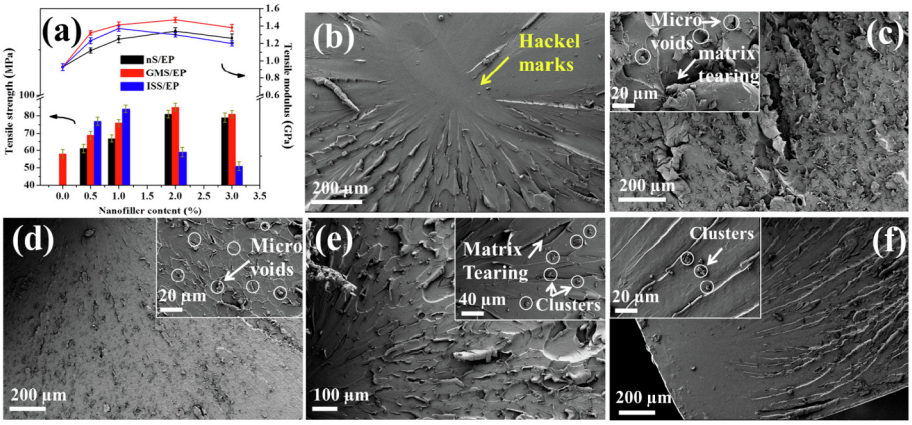

Fig. 6. (a) Tensile properties of epoxy nanocomposites at varying contents of nS, GMS and ISS nanoparticles. Microscopic tensile fracture surfaces of epoxy nanocomposites (b) neat epoxy (EP) (c) nS/EP-1 (d) GMS/EP-1 and (e) ISS/EP-1 and (f) ISS/EP-2.

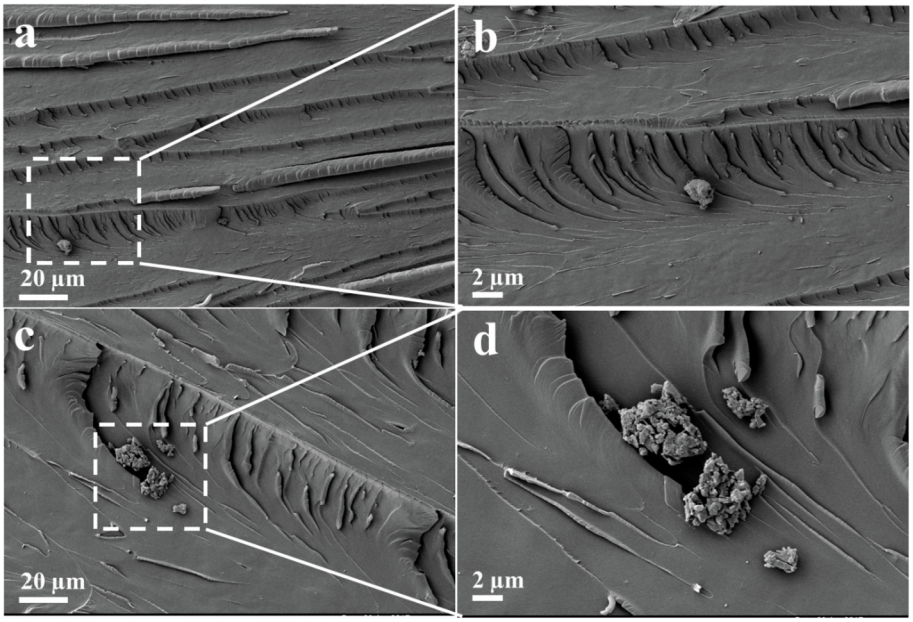

Fig. 7. High magnification FESEM images of fracture surfaces taken from tensile specimens of the composites filled with (a, b) 1 wt% ISS (c, d) 2 wt% ISS.

added epoxy nanocomposites (nS/EP) system, the tensile strength as well as the tensile modulus increases with the increase in nanoparticle content. The maximum tensile strength of ~81 MPa and tensile modulus of ~1.34 GPa is found after 2 wt % of nS addition in the epoxy system. This leads to ~39% and ~34% enhancement in tensile strength and tensile modulus than that of the EP. The epoxy nanocomposites having GMS (GMS/EP) shows enhancement of ~45.6% (~85 MPa) in tensile strength and ~46.5% (~1.48 GPa) in modulus with respect to the EP when 2 wt % of reinforcement is done. In contrast, the maximum increment in tensile strength and tensile modulus for ISS added epoxy nanocomposites (ISS/EP) is found after 1 wt % of reinforcement. The enhancement in tensile strength and tensile modulus for ISS/EP-1 is found as ~45% (~84 MPa) and ~36% (~1.37 GPa) with respect to the EP system respectively. This is mainly ascribed to the cross-linking capability of the imidazole group present on the surfaces of the ISS to enhance the interfacial properties [51]. Further increase of ISS contents (> 1 wt %) reduces both tensile strength and tensile modulus dramatically, which may be attributed to the agglomeration of ISS in epoxy system. However, due to hydrophobic nature of GMS, the generation of an efficient creating interphase due to the covalent bonding between hydroxyl group of GMS and epoxide network lead to homogeneous dispersion in the matrix system. By increasing particle content (> 2 wt % of GMS), the tensile strength and modulus start decreases. This may be attributed to the excess covalent attachment of organic moieties on GMS particles may inhibit the curing reaction rate and dominant the crosslinking density [52]. On the other hand, relatively high degree of covalent attachment or high wt % of particle loading may cause a clogging effect leads to generation of weak structure of cross-linking network. Similar trend is also reported by others wherein they demonstrated that GO coating on silica particle can largely enhance the mechanical properties of epoxy composites. Located at the interface, the GO shells on silica surface could serve as influential coupling agent for the modification of silica particles, leading to a significant enhancement of interfacial interactions [53] in the matrix system.

The tensile fracture surface of EP, nS/EP, GMS/EP and ISS/EP was investigated under FESEM and is demonstrated in Fig. 6(b–f). The fractography surface of neat epoxy (EP) shows a smooth surface with hackles markings suggesting brittle fracture as shown in Fig. 6 (b). The fractography of nanocomposites containing 1 wt % of nS demonstrates rougher fracture surface throughout as can be seen in Fig. 6 (c). This might be due to poorly adhered large sized particles that leads to the increases in the surface roughness with insignificant plastic deformation [54]. High magnification FESEM investigation (top left corner in Fig. 6 (c)) for nS/EP shows presence of micron sized voids (white encircled) with large scale matrix tearing (marked by white arrow), indicating crack path deflection that somehow contributes towards tensile performance enhancement. Fig. 6 (d) shows the tensile fracture surfaces of composites containing 1 wt % of GMS nanoparticles. A comparatively smoother fracture surface indicates better adhesion of the GMS nanoparticles with the epoxy matrix. Higher magnification fractography of GMS/EP reveals multiple sites for striation formation and propagation suggesting better dispersion of the GMS nanoparticles within the epoxy matrix as can be seen in top right corner in Fig. 6 (d). In addition, places are found wherein mico voids (marked with white arrow) are grown where crack is pinned because of the tailored interfacial stiffness at the juncture of the GMS nanoparticles and the matrix. For ISS/EP having 1 wt % of ISS, a comparatively rougher fracture surface is demonstrated after examining under FESEM at low magnification as can be seen in Fig. 6 (e). This enhanced matrix tearing effect with the reduction in the formation of striations elucidates brittleness in the system. After examining under FESEM at high magnification as demonstrated in the top right corner in Fig. 6 (e), we found un-adhered/partially adhered clusters and matrix tearing marks. However, since these cluster size is smaller than that of the nS/EP the tensile performance of ISS/EP is improved. This behavior is found more prominent for ISS/EP having 2 wt % of ISS, where in further smoother fracture surface along with big sized agglomeration is found as can be seen in Fig. 6 (f).

3.4. Interface and microstructure in the nanocomposites

In order to further understand the influence of ISS on the ISS/matrix interfacial quality, high magnification FESEM fracture surface investigation of the composites filled with 1 and 2 wt % ISS after tensile tests has been performed and is shown in Fig. 7(a–d).

The fracture surface of the composites having 1 wt% of ISS shows finer river-like structures Fig. 7 (a). The enlarged view as shown in Fig. 7(b) shows well-embedded non-aggregated ISS nanoparticles in the epoxy matrix that led to the crack propagation around the particles. This indicates a better interfacial stiffness of the ISS/matrix system after imidazole functionalization. Consequently, increases the load

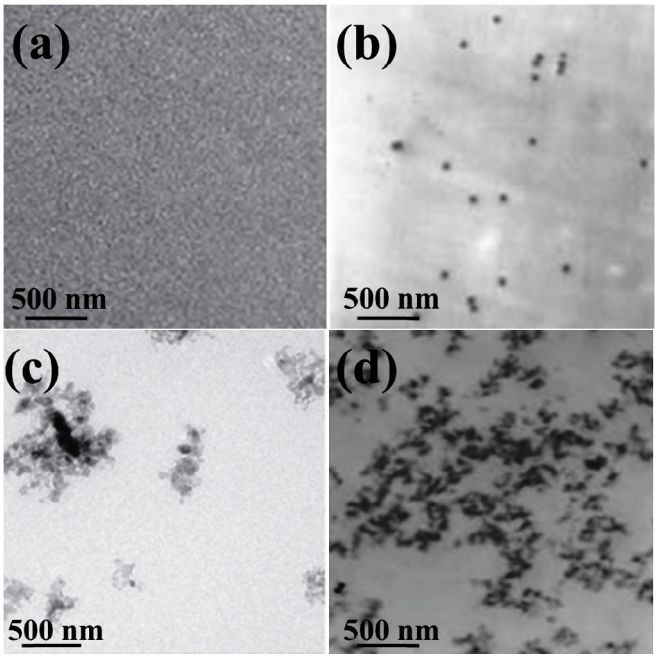

Fig. 8. Dispersion study of ISS particle in epoxy system (a) neat epoxy (b) 1 wt % ISS (c) 2 wt % ISS and (d) 3 wt % ISS.

transferring ability of the matrix polymer [55,56]. For the ISS/EP-2 nanocomposites, the low magnification FESEM image demonstrates aggregates of ISS as shown in Fig. 7 (c). Such aggregates of ISS may hinder the modification of the interfacial stiffness and can create stress concentration zones during the fracture process, impairing stress transfer ability of the matrix.

The dispersion analysis of the ISS/epoxy composites under TEM revealed aggregation of the ISS nanoparticles at higher weight fraction. Fig. 8(a–d) shows TEM micrographs for ISS/EP system with the increase in the nanoparticle content. A homogeneous distribution is observed till 1 wt % of ISS nanoparticles is reinforced in the epoxy system. However, at higher nanoparticle content (> 2 wt %) sites with large extent of aggregated ISS nanoparticle can be seen. It was expected that the presence of organic moieties on the ISS surfaces has capability to influence homogeneous distribution within the epoxy system, but possibly the GPTMS linker on the ISS nanoparticles provides dual functionality [57]. First and prime function is to stabilize the silica colloids in the epoxy matrix system and other is to provide chemical interactions with the curing agent (HY906). The surface energy of ISS at lower wt % might be low due to the stabilization along with chemical interaction of ISS with the matrix ingredients that led to the reduction in agglomeration tendency in the epoxy matrix system. Whereas, reinforcement of more than 2 wt % of ISS in epoxy system may provide chemical interactions of ISS particles amongst themselves on large scale due to formation of H-bonding from hydroxyl groups present on the surfaces of ISS nanoparticles, which may increases the clustering tendency.

3.5. Fracture properties of nanocomposites

The fracture resistance of epoxy nanocomposites containing modified and unmodified silica (0.5, 1, 2 and 3 wt %) was investigated from SENB test and the result obtained is shown in Fig. 9.

The value of K_{IC} and G_{IC} for neat epoxy (EP) is ~0.62 MPa $m^{0.5}$ and ~400 J m^{-2} respectively. The K_{IC} and G_{IC} for nS/EP are found maximum at 2 wt % of addition. Significant increment in K_{IC} and G_{IC} is found for GMS/EP in comparison to EP. There was ~32% (1 MPa $m^{0.5}$) and ~67% (666 J m^{-2}) improvement of K_{IC} and G_{IC} is noted when 2 wt % of GMS is added. In contrast, for ISS/EP system maximum improvement of K_{IC} and G_{IC} is observed at low filler addition i.e. 1 wt % in comparison to the other variants. The improvement found is ~25% (0.95 MPa $m^{0.5}$) and ~46% (585 J m^{-2}) higher than that of the EP and is in well comparable to GMS/EP system. Further addition of ISS nanoparticles up to 3 wt %, diminishes the K_{IC} and G_{IC} value. Similar results were reported elsewhere for functionalized silica/epoxy nanocomposites [58].

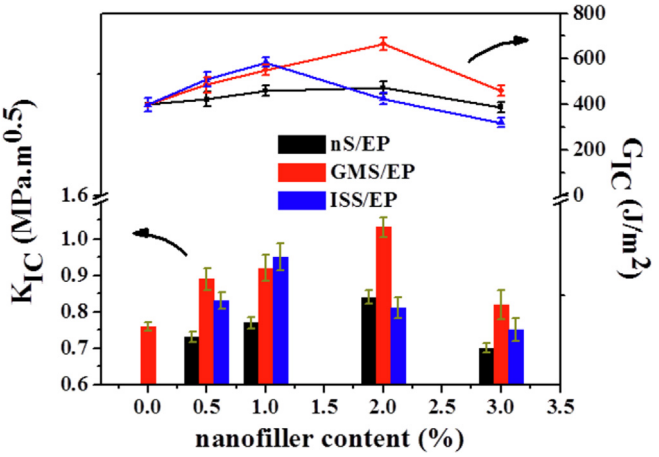

Fig. 9. Fracture properties of epoxy nanocomposites at varying contents of nS, GMS and ISS nanoparticles.

3.6. Morphological analysis of mode-I fracture surfaces

Failure modes of the epoxy nanocomposites under three point notched bend test primarily depends on various factors, such as stress concentration zone, crack propagation path, stress transfer from matrix to filler and the particle debonding [59].

Schematic representation for the stress conditions and possible failure modes during crack propagation for nS/EP and GMS/EP as well as ISS/EP system is shown in Fig. 10. It is considered that the compressive region of the nanocomposites bear local crushing at the same time the tensile region tended to initiate crack propagation under the application of transverse load. However, the local stress concentration site mainly originates at the neck region due to matrix failure that leads to failure. In present study, the fracture resistance of nanocomposites was significantly influenced by GMS or ISS nanoparticle. Since the GMS and ISS epoxy nanocomposites possesses high tensile modulus enhances the load carrying capability till the stress level that exceeds the K_{IC} of EP (0.76 MPa $m^{0.5}$). Hence, the propagation of cracks for GMS/EP as well as ISS/EP is expected to be delayed due to better dispersion of nanoparticles.

In order to understand the fracture behavior of the nanocomposites systems, fractography analysis for neat epoxy, nanocomposites filled with unmodified and modified silica at 1 wt % particle contents was conducted under FESEM (Fig. 11(a–c)). The fracture surface of the neat epoxy (Fig. 11 (a)) is found smooth (indicated by white arrow in Fig.) along with river patterns depicting brittle failure. However, for nS/EP-1, localized shear yielding zones in the form of shear bands and river lines are found (Fig. 11 (b)). These zones may restrict the crack propagation resulting in absorption of more energy prior to failure of the material. On the other hand, the fracture surfaces of ISS/EP-1 specimens is found to have a comparative rougher fracture surface along with the craze lines (micro cracks) indicating matrix plastic deformation (Fig. 11 (c)). This increased number of craze lines for ISS/EP-1 and therefore the fracture surface roughness justifies the enhanced fracture toughness of ISS/EP as compared to the nS/EP [60,61]. This feature indicates slow crack propagation due to the absorption of more energy for the restriction towards new fracture surface creation.

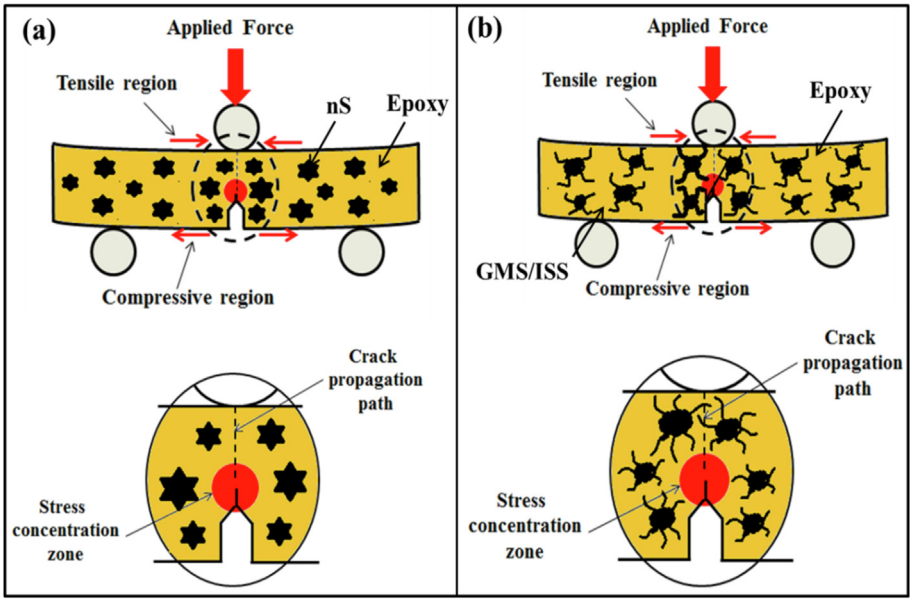

Fig. 10. Schematic representation for the crack propagation in three point notched bend samples (a) nS/EP and (b) ISS/EP nanocomposites.

4. Conclusion

GMS as well as ISS nanoparticles were facilely prepared from TEOS precursor by co-condensation method via one-pot sol-gel processing. Surface functionalization of silica was confirmed from spectroscopic analysis and their thermal degradation behavior. The FTIR as well as XPS analysis demonstrates the presence of imidazole moiety on the surface of nS. Both GMS as well ISS nanoparticles uplifts the tensile performance of the epoxy nanocomposites system. The GMS/EP enhances the tensile strength as well as the tensile modulus by ~45% and ~46% with respect to the neat epoxy (EP). For the ISS/EP system similar enhancement is achieved as lower filler content. Although fracture toughness as well as fracture energy was significantly higher for GMS/EP in comparison to EP, but ISS/EP shows a well comparable results interestingly at low filler content. The fracture analysis reveals well dispersed GMS nanoparticles in epoxy system generates micro voids that pined the crack along its pathway thereby absorbs more energy prior to failure. For ISS/EP system the tendency of the ISS nanoparticles to attract amongst themselves hinders the better adherence with the epoxy system to modulate the stiffness at the juncture of the matrix and the particle at higher filler content. These noticeable improvement offered by both GMS as well as ISS opens up the scope to use theses on-pot synthesized nanoparticles as toughness enhancer for highly brittle epoxy systems.

Acknowledgement

The authors thank the Department of Science and Technology, India under DST-FIST program 2014 with Grant No: SR/FST/ETI-373/2014. The authors also want to thank NMHS project with Grant No: NMHS/2016–2017/SG 18/07 for financial support. This work was initiated under the project head "Synthesis and Fracture Property Evaluation of

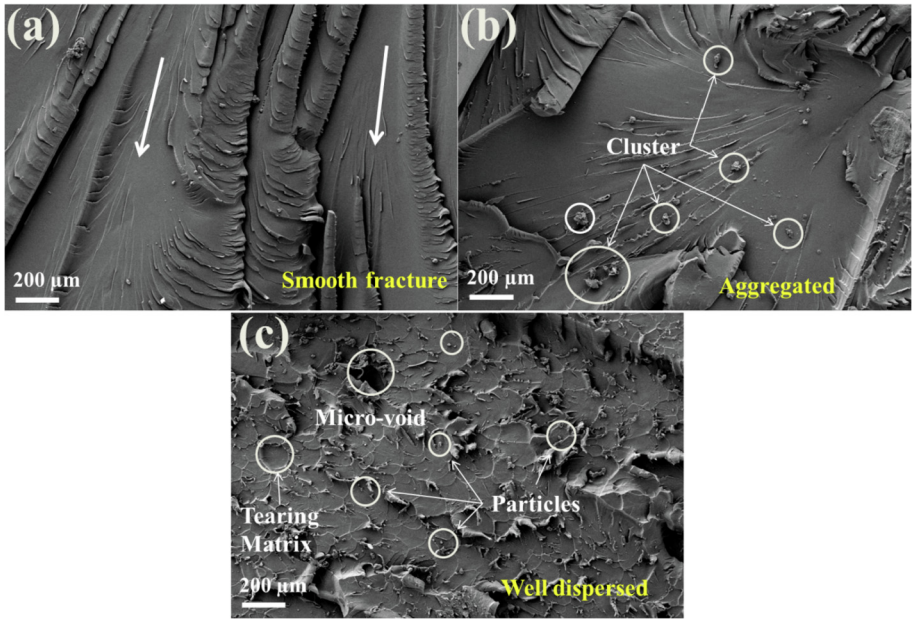

Fig. 11. FESEM micrographs showing the failure mechanisms of the fracture surface obtained from the 3-point bending specimens (a) Neat epoxy (EP) (b) nS/EP-1 and (c) ISS/EP-1 nanocomposites.

Polymer Nanocomposites" supported by National Institute of Technology Silchar, Assam, India (Project number (RC)/457/122).

References

[1] P. Mohan, A critical review: the modification, properties, and applications of epoxy resins, Polym. Plast. Technol. Eng. 52 (2013) 107–125, https://doi.org/10.1080/03602559.2012.727057.

[2] J. Townsend, R. Burtovyy, P. Aprelev, K.G. Kornev, I. Luzinov, Enhancing mechanical and thermal properties of epoxy nanocomposites via alignment of magnetized SiC whiskers, ACS Appl. Mater. Interfaces 9 (2017) 22927–22940, https://doi.org/10.1021/acsami.7b04546.

[3] M.Z. Rong, M.Q. Zhang, W.H. Ruan, Surface modification of nanoscale fillers for improving properties of polymer nanocomposites: a review, Mater. Sci. Technol. 22 (2006) 787–796, https://doi.org/10.1179/174328406X101247.

[4] A.G. Koniuszewska, J.W. Kaczmar, Application of polymer based composite materials in transportation, Progress in Rubber, Plastics. Recycl. Technol. 32 (2016) 1–24 http://0-search.ebscohost.com.oak.indwes.edu/login.aspx?direct=true&db=a9h&AN=113037648&site=eds-live.

[5] F. Hussain, M. Hojjati, M. Okamoto, R.E. Gorga, Review article: polymer-matrix nanocomposites, processing, manufacturing, and application: an overview, J. Compos. Mater. 40 (2006) 1511–1575, https://doi.org/10.1177/0021998306067321.

[6] H. Gu, C. Ma, J. Gu, J. Guo, X. Yan, J. Huang, Q. Zhang, Z. Guo, An overview of multifunctional epoxy nanocomposites, J. Mater. Chem. C 4 (2016) 5890–5906, https://doi.org/10.1039/c6tc01210h.

[7] B.B. Johnsen, A.J. Kinloch, R.D. Mohammed, A.C. Taylor, S. Sprenger, Toughening mechanisms of nanoparticle-modified epoxy polymers, Polymer 48 (2007) 530–541, https://doi.org/10.1016/j.polymer.2006.11.038.

[8] S. Haldera, P.K. Ghosh, M.S. Goyat, S. Ray, Ultrasonic dual mode mixing and its effect on tensile properties of SiO2-epoxy nanocomposite, J. Adhes. Sci. Technol. 27 (2013) 111–124, https://doi.org/10.1080/01694243.2012.701510.

[9] S. Halder, T. Prasad, N.I. Khan, M.S. Goyat, S. Ram Chauhan, Superior mechanical properties of poly vinyl alcohol-assisted ZnO nanoparticle reinforced epoxy composites, Mater. Chem. Phys. 192 (2017) 198–209, https://doi.org/10.1016/j.matchemphys.2016.12.055.

[10] T. Prasad, S. Halder, M.S. Goyat, S.S. Dhar, Morphological dissimilarities of ZnO nanoparticles and its effect on thermo-physical behavior of epoxy composites, Polym. Polym. Compos. 39 (2018) 135–145, https://doi.org/10.1002/pc.

[11] M. AC, R. B, Effect of zinc oxide nanoparticles on mechanical properties of diglycidyl ether of bisphenol-A, J. Mater. Sci. Eng. 05 (2016), https://doi.org/10.4172/2169-0022.1000291.

[12] O. Zabihi, M. Ahmadi, H. Khayyam, M. Naebe, Fish DNA-modified clays: towards highly flame retardant polymer nanocomposite with improved interfacial and mechanical performance, Sci. Rep. 6 (2016) 1–17, https://doi.org/10.1038/srep38194.

[13] C. Velasco-santos, A.L. Martı, R. Ruoff, V.M. Castan, Improvement of thermal and mechanical properties of carbon nanotube composites through chemical functionalization, Chem. Mater. 15 (2003) 4470–4475.

[14] Y. Zhang, S. Huang, Significant improvements in the mechanical properties of chitosan functionalized carbon nanotubes/epoxy composites, RSC Adv. 6 (2016) 26210–26215, https://doi.org/10.1039/c6ra00597g.

[15] Y. Ni, L. Chen, K. Teng, J. Shi, X. Qian, Z. Xu, X. Tian, C. Hu, M. Ma, Superior mechanical properties of epoxy composites reinforced by 3D interconnected graphene skeleton, ACS Appl. Mater. Interfaces 7 (2015) 11583–11591, https://doi.org/10.1021/acsami.5b02552.

[16] K.S. Khare, F. Khabaz, R. Khare, Effect of carbon nanotube functionalization on mechanical and thermal properties of cross-linked epoxy − carbon nanotube Nanocomposites : role of strengthening the interfacial interactions, ACS Appl. Mater. Interfaces 6 (2014) 6098–6110, https://doi.org/10.1021/am405317x.

[17] M. Yoonessi, M. Lebrón-Colón, D. Scheiman, M.A. Meador, Carbon nanotube epoxy nanocomposites: the effects of interfacial modifications on the dynamic mechanical properties of the nanocomposites, ACS Appl. Mater. Interfaces 6 (2014) 16621–16630, https://doi.org/10.1021/am5056849.

[18] M.S. Goyat, S. Rana, S. Halder, P.K. Ghosh, Facile fabrication of epoxy-TiO 2 nanocomposites: a critical analysis of TiO 2 impact on mechanical properties and toughening mechanisms, Ultrason. Sonochem. 40 (2018) 861–873, https://doi.org/10.1016/j.ultsonch.2017.07.040.

[19] E.S.A. Rashid, M.F.A. Rasyid, H.M. Akil, K. Ariffin, C.C. Kooi, Effect of (3-aminopropyl) triethylsilane treatment on mechanical and thermal properties of alumina-filled epoxy composites, Proc. IME J. Mater. Des. Appl. 225 (2011) 160–170, https://doi.org/10.1177/0954420711403214.

[20] S. Halder, P.K. Ghosh, M.S. Goyat, Influence of ultrasonic dual mode mixing on morphology and mechanical properties of ZrO2-epoxy nanocomposite, High Perform. Polym. 24 (2012) 331–341.

[21] H. Zou, S. Wu, J. Shen, Polymer/silica nanocomposites: preparation, characterization, properties, and applications, Chem. Rev. 108 (2008) 3893–3957.

[22] S.-Y. Fu, X.-Q. Feng, B. Lauke, Y.-W. Mai, Effect of partcle size, particle/matrix interface adhesion and particle loadingon mechanical properties of particulate-polymer composites, Composites Part B (2008) 933–961.

[23] M. Conradi, G. Intihar, M. Zorko, Mechanical and wetting properties of nanosilica/epoxy-coated stainless steel, Mater. Technol. 49 (2015) 613–618, https://doi.org/10.17222/mit.2015.060.

[24] C. Alzina, N. Sbirrazzuoli, A. Mija, Eppxy-Amine based nanocomposites reinforced by silca nanoparticles. Relatioship between morphologic aspect, cure kinetics, and thermal properties, J. Phys. Chem. C 115 (2011) 22789–22795.

[25] H. Behniafar, M.K. Nazemi, Effect of amine-functionalized silica nanoparticles on thermal and mechanical behaviors of DGEBA/IPD epoxy networks, Polym. Bull. 74 (2017) 3739–3749, https://doi.org/10.1007/s00289-017-1928-z.

[26] W. Han, Y. Yu, L. Fang, M.R. Johnston, Z.Q. Shi, Y. Tang, Functionalized silica-epoxy nanocomposites with enhanced fracture toughness for large scale applications, J. Compos. Mater. 49 (2015) 1439–1447.

[27] M. Conradi, M. Zorko, A. Kocijan, I. Verpoest, Mechanical properties of epoxy composites reinforced witha low volume fraction of nanosilica fillers, Mater. Chem. Phys. 137 (2013) 910–915.

[28] W. Liu, K.L. Koh, J. Lu, L. Yang, S. Phua, J. Kong, Z. Chen, X. Lu, Simultaneous catalyzing and reinforcing effects of imidazole-functionalized graphene in anhydride-cured epoxies, J. Mater. Chem. 22 (2012) 18395–18402, https://doi.org/10.1039/c2jm32708b.

[29] Q. Lyu, H. Yan, L. Li, Z. Chen, H. Yao, Y. Nie, Imidazolium ionic liquid modified graphene oxide: as a reinforcing filler and catalyst in epoxy resin, Polymers 447 (2017) 1–15, https://doi.org/10.3390/polym9090447.

[30] C. Zhang, X. Mi, J. Tian, J. Zhang, T. Xu, Supported ionic liquid silica as curing agent for epoxy composites with improved mechanical and thermal properties, Polymers 478 (2017) 1–11, https://doi.org/10.3390/polym9100478.

[31] A. Paula, A. Carvalho, B.G. Soares, S. Livi, Organically modified silica (ORMOSIL) bearing imidazolium – based ionic liquid prepared by hydrolysis/co-condensation of silane precursors: synthesis, characterization and use in epoxy networks, Eur. Polym. J. 83 (2016) 311–322, https://doi.org/10.1016/j.eurpolymj.2016.08.030.

[32] Y. Yin, R. Huang, Y. Xu, C. Wang, Preparation and characterization of highly dispersed silica nanoparticles via nonsurfactant template for fabric coating, J. Text. Inst. 108 (2017) 1662–1668, https://doi.org/10.1080/00405000.2017.1278999.

[33] K. Wang, J. Wu, L. Chen, C. He, M. Toh, Epoxy nanocomposites with highly exfoliated pristine clay: mechanical properties and fracture mechanism, Macromolecules 38 (2005) 788–800.

[34] T. Matsoukas, E. Gulari, Monomer-addition growth with a slow initiation Step : a growth model for silica particles from alkoxides, J. Colloid Interface Sci. 132 (1989) 13–21.

[35] R.P. Bagwe, L.R. Hilliard, W. Tan, Surface modification of silica nanoparticles to reduce aggregation and nonspecific binding surface modification of silica nanoparticles to reduce aggregation and nonspecific binding, Langmuir 22 (2006) 4357–4362, https://doi.org/10.1021/la052797j.

[36] P. Innocenzi, C. Figus, T. Kidchob, M. Valentini, B. Alonso, M. Takahashi, Sol-gel reactions of 3-glycidoxypropyltrimethoxysilane in a highly basic aqueous solution, J. Chem. Soc. Dalton Trans. (2009) 9146–9152, https://doi.org/10.1039/b905830c.

[37] Y. Zhou, K. Shimizu, J.N. Cha, G.D. Stucky, D.E. Morse, Efficient catalysis of polysiloxane synthesis, Angew. Chem. Int. Ed. 38 (1999) 779–782, https://doi.org/10.1002/(SICI)1521-3773(19990315)38 6 < 779::AID-ANIE779 > 3.0.CO;2-#.

[38] M. Perchacz, R.K. Donato, L. Seixas, A. Zhingunow, R. Konefal, M. Serkis-Rodzen, H. Benes, Ionic Liquid-Silica Precursors via Solvent-Free Sol – Gel Process and their application in epoxy-amine network: a theoretical/experimental study, Applied Materials and Interface (2017), https://doi.org/10.1021/acsami.7b02631.

[39] M.-Y. han, W.Y.Y. Han, Z. Lu, Z. Teng, J. Liang, Z. Guo, D. Wang, Unravelling the growth mechanism of silica particles in stober method: in situ seeded growth model, Langmuir 33 (2017) 5879–5890, https://doi.org/10.1021/acs.langmuir.7b01140.

[40] A. Liberman, N. Mendez, W.C. Trogler, A.C. Kummel, Synthesis and surface functionalization of silica nanoparticles for nanomedicine, Surf. Sci. Rep. 69 (2015) 132–158, https://doi.org/10.1016/j.surfrep.2014.07.001.Synthesis.

[41] I.A. Rahman, P. Vejayakumaran, C.S. Sipaut, J. Ismail, M.A. Bakar, R. Adnan, C.K. Chee, An optimized sol-gel synthesis of stable primary equivalent silica particles, Colloid. Surf. Physicochem. Eng. Asp. 294 (2007) 102–110, https://doi.org/10.1016/j.colsurfa.2006.08.001.

[42] Y. Lu, X. Yan, An imprinted organic-inorganic hybrid sorbent for selective separation of cadmium from aqueous solution an imprinted organic - inorganic hybrid sorbent for selective separation of cadmium from aqueous, Anal. Chem. 76 (2017) 453–457, https://doi.org/10.1021/ac0347718.

[43] P. Innocenzi, G. Brusatin, M. Guglielmi, R. Bertani, New synthesis rout to 3 (Glycidoxypropyl) trimethoxysilane-based hybrid organic-inorganic materials, Chem. Mater. 11 (1999) 1672–1679.

[44] Z. Wang, C. Ye, X. Wang, J. Li, Adsorption and desorption characteristics of imidazole-modified silica for chromium(VI), Appl. Surf. Sci. 287 (2013) 232–241, https://doi.org/10.1016/j.apsusc.2013.09.133.

[45] Z. Al Othman, A.W. Apblett, Synthesis of mesoporous silica grafted with 3-glycidoxypropyltrimethoxy-silane, Mater. Lett. 63 (2009) 2331–2334, https://doi.org/10.1016/j.matlet.2009.07.067.

[46] Y. Wang, T. Zhu, K.H. Row, Preparation and evaluation of silica-based ionic liquid-modified stationary phase for HPLC, J. Chromatogr. Sci. 48 (2010) 690–693, https://doi.org/10.1093/chromsci/48.8.690.

[47] W. He, D. Wu, J. Li, K. Zhang, Y. Xiang, L. Long, S. Qin, J. Yu, Q. Zhang, Surface modification of colloidal silica nanoparticles: controlling the size and grafting process, Bull. Korean Chem. Soc. 34 (2013) 2747–2752, https://doi.org/10.5012/bkcs.2013.34.9.2747.

[48] S.S. Jedlicka, J.L. Rickus, D.Y. Zemlyanov, Surface analysis by X-ray photoelectron spectroscopy of sol - gel silica modified with covalently bound peptides, J. Phys. Chem. B 111 (2007) 11850–11857.

[49] Y. Lin, S. Liu, J. Peng, L. Liu, The filler – rubber interface and reinforcement in styrene butadiene rubber composites with graphene/silica hybrids : a quantitative correlation with the constrained region, Composites Part A 86 (2016) 19–30.

[50] J. Ettehadi, A. Shakeri, H. Sid, Synthesis and characterization of silica – polyvinyl

imidazole core – shell nanoparticles via combination of RAFT polymerization and grafting-to method, Polymer Advance Technology 28 (2017) 1884–1891, https://doi.org/10.1002/pat.4077.
[51] K. Maghsoudi, S. Motahari, Mechanical, thermal and hydrophobic propertiws of silica aerogel-epoxy composites, J. Appl. Polym. Sci. (2018) 1–9, https://doi.org/10.1002/APP 45706.
[52] V.A. Online, Toward e ff ective and tunable interphases in graphene oxide/epoxy composites by grafting di ff erent chain lengths of polyetheramine onto graphene oxide †, (2014), pp. 15058–15069, https://doi.org/10.1039/c4ta02429j.
[53] L. Chen, S. Chai, K. Liu, N. Ning, J. Gao, Q. Liu, F. Chen, Q. Fu, Enhanced epoxy/silica composites mechanical properties by introducing graphene oxide to the interface, ACS Appl. Mater. Interfaces 4 (2012) 4398–4404.
[54] I. Zaman, B. Manshoor, A. Khalid, Q. Meng, S. Arabey, Interface modification of clay and graphene platelets reinforced epoxy nanocomposites: a comparative study, J. Mater. Sci. 49 (2014) 5856–5865.
[55] H. Xu, L. Gong, X. Wang, L. Zhao, Y. Pei, G. Wang, Y. Liu, L. Wu, J. Jiang, L. Tang, Composites : Part A Influence of processing conditions on dispersion, Elect. Mech. Prop. Graph. Filled-Silicone Rub. Comp. 91 (2016) 53–64.
[56] L. Gong, Y. Pei, Q. Han, L. Zhao, L. Wu, J. Jiang, L. Tang, Polymer Grafted Reduced Graphene Oxide Sheets for Improving Stress Transfer in Polymer Composites vol. 134, (2016), pp. 144–152.
[57] M.G. Veena, N.M. Renukappa, K. n Shivkumar, S. Seetharamu, Dielectric properties of nanosilica filled epoxy nanocomposites, Indian Aca. Sci. 41 (2016) 407–414.
[58] W. Han, Y. Yu, L. Fang, M.R. Johnston, S.Z. Qiao, Y. Tang, Functionalised silica/epoxy nanocomposites with enhanced fracture toughness for large-scale applications, J. Compos. Mater. 49 (2015) 1439–1447, https://doi.org/10.1177/0021998314534867.
[59] M.R. Zakaria, M.H.A. Kudus, H.M. Akil, M.H. Zamri, Improvent of fracture toughness in epoxy nanocomposites through chemical hybridization of carbon nanotubes and alumina, Materials 10 (2017) 1–11, https://doi.org/10.3390/ma10030301.
[60] M. Zappalorto, M. Salviato, M. Quaresimin, Mixed Mode (I + II) Fracture Toughness of Polymer Nanoclay Nanocomposites vol. 111, (2013), pp. 50–64.
[61] M. Albdiry, B. Yousif, Toughening of brittle polyster with functionalized hallosite nanocomposites, Composites Part B 160 (2019) 94–109.